ISSN 1674-1056
http://cpb.iphy.ac.cn
http://iopscience.iop.org/cpb
中国物理 B
Chinese Physics
中国物理 Chinese Physics B

Thermoelectric properties of two-dimensional hexagonal indium-VA

Jing-Yun Bi(毕京云), Li-Hong Han(韩利红), Qian Wang(王倩), Li-Yuan Wu(伍力源), Ruge Quhe(屈贺如歌), Peng-Fei Lu(芦鹏飞)
Citation: Chin. Phys. B . 2018, 27(2): 026802. **doi:** 10.1088/1674-1056/27/2/026802

Journal homepage: http://cpb.iphy.ac.cn; http://iopscience.iop.org/cpb

What follows is a list of articles you may be interested in

Photodetecting and light-emitting devices based on two-dimensional materials

Yuanfang Yu(于远方), Feng Miao(缪峰), Jun He(何军), Zhenhua Ni(倪振华)
Chin. Phys. B . 2017, 26(3): 036801. **doi:** 10.1088/1674-1056/26/3/036801

A review for compact model of graphene field-effect transistors

Nianduan Lu(卢年端), Lingfei Wang(汪令飞), Ling Li(李泠), Ming Liu(刘明)
Chin. Phys. B . 2017, 26(3): 036804. **doi:** 10.1088/1674-1056/26/3/036804

Growth condition optimization and mobility enhancement through inserting AlAs monolayer in the InP-based $In_xGa_{1-x}As/In_{0.52}Al_{0.48}As$ HEMT structures

Shu-Xing Zhou(周书星), Ming Qi(齐鸣), Li-Kun Ai(艾立鹍), An-Huai Xu(徐安怀)
Chin. Phys. B . 2016, 25(9): 096801. **doi:** 10.1088/1674-1056/25/9/096801

In-plane anisotropy in two-dimensional electron gas at $LaAlO_3/SrTiO_3$(110) interface

Sheng-Chun Shen(沈胜春), Yan-Peng Hong(洪彦鹏), Cheng-Jian Li(厉承剑), Hong-Xia Xue(薛红霞), Xin-Xin Wang(王欣欣), Jia-Cai Nie(聂家财)
Chin. Phys. B . 2016, 25(7): 076802. **doi:** 10.1088/1674-1056/25/7/076802

Growth condition optimization and mobility enhancement throughprolonging the GaN nuclei coalescence process of AlGaN/AlN/GaN structure

He Xiao-Guang, Zhao De-Gang, Jiang De-Sheng, Zhu Jian-Jun, Chen Ping, Liu Zong-Shun, Le Ling-Cong, Yang Jing, Li Xiao-Jing, Zhang Shu-Ming, Yang Hui
Chin. Phys. B . 2015, 24(9): 096802. **doi:** 10.1088/1674-1056/24/9/096802

Thermoelectric properties of two-dimensional hexagonal indium–VA*

Jing-Yun Bi(毕京云)[1], Li-Hong Han(韩利红)[1], Qian Wang(王倩)[1], Li-Yuan Wu(伍力源)[1], Ruge Quhe(屈贺如歌)[1,2,†], and Peng-Fei Lu(芦鹏飞)[1,3,‡]

[1] State Key Laboratory of Information Photonics and Optical Communications, Beijing University of Posts and Telecommunications, Beijing 100876, China
[2] School of Science, Beijing University of Posts and Telecommunications, Beijing 100876, China
[3] State Key Laboratory of Functional Materials for Informatics, Shanghai Institute of Microsystem and Information Technology, Chinese Academy of Sciences, Shanghai 200050, China

(Received 6 September 2017; revised manuscript received 4 November 2017; published online 5 January 2018)

The electrical properties and thermoelectric (TE) properties of monolayer In–VA are investigated theoretically by combining first-principles method with Boltzmann transport theory. The ultralow intrinsic thermal conductivities of 2.64 $W\cdot m^{-1}\cdot K^{-1}$ (InP), 1.31 $W\cdot m^{-1}\cdot K^{-1}$ (InAs), 0.87 $W\cdot m^{-1}\cdot K^{-1}$ (InSb), and 0.62 $W\cdot m^{-1}K^{-1}$ (InBi) evaluated at room temperature are close to typical thermal conductivity values of good TE materials ($\kappa < 2\ W\cdot m^{-1}\cdot K^{-1}$). The maximal ZT values of 0.779, 0.583, 0.696, 0.727, and 0.373 for InN, InP, InAs, InSb, and InBi at p-type level are calculated at 900 K, which makes In–VA potential TE material working at medium-high temperature.

Keywords: thermoelectric properties, two-dimensional In–VA, figure of merit

PACS: 68.65.–k, 63.22.–m, 73.40.Kp, 84.60.Bk **DOI:** 10.1088/1674-1056/27/2/026802

1. Introduction

Motivated by graphene,[1] one has taken a great interest in other two-dimensional (2D) layered materials, such as hexagonal boron nitride (h-BN),[2,3] black phosphorus,[4–6] silicene,[7,8] and stanene.[9] The 2D materials often present novel and versatile electronic, optical, and mechanical properties, which make them useful in fundamental science and engineering applications. In particular, due to their unexceptionable electrical and thermal transport properties, 2D materials have shown great potential applications in thermal management, thermoelectric (TE) energy generation, and heat-to-electricity conversion.[10]

The TE properties of materials are characterized by the TE figure of merit ZT, which is defined as $ZT = \sigma S^2 T/\kappa_e + \kappa_l$, where σ is the electric conductivity, S is the Seebeck coefficient, T is the absolute temperature, κ_e and κ_l are the electronic and lattice thermal conductivity, respectively. The power factor is defined as $PF = \sigma S^2$, which characterizes electric power output. Large ZT values for TE materials are significant for practical device applications. In 2007, Dragoman D and Dragoman M put forward graphene as TE material[11] with a maximum S value of 30 mV/K. After that, the potentials of 2D allotropes of group-IV (silicene, germanene, stanene) and group-V (arsenene, black and blue phosphorus) materials[12,13] for TE applications have also been explored.

Due to an extensive range of direct band gaps and stability at high temperature, the III–V compound semiconductor family is one of the most commonly used groups of semiconductors. Bulk III–nitrides have been receiving attention as potential high-temperature TE materials.[14–19] Their thin films[20] and thin-film-based nanostructures[21] have shown enhanced in-plane TE conductivity compared with that of the corresponding bulks. An unprecedented high ZT of 1.28 at 773 K was obtained in the InSb-based alloys by optimizing the eutectic content.[22] Recently, a large number of 2D materials in group III–V family, such as AlN, GaN, and InAs, have been predicted to be structurally stable.[23–25] Experimentally, 2D H-BN[26] and h-AlN[27] have been fabricated, impelling the research of 2D III–V materials. Huang *et al.*[28] studied the relative peak power factors of group-III nitride (BN, AlN, and GaN) atomic sheets under strain. Among 2D group III–V materials, indium-VA possesses the smallest effective mass and the highest electron mobility, which could cause large electronic conductivities and high ZT.

While previous efforts focused on the structural and electronic properties of 2D III–V materials, TE properties of these materials are seldom studied. Therefore, in this paper, the structural, electronic, phonon and TE properties of 2D In–VA compound are investigated by first-principles method combining with Boltzmann transport approach. Among 2D In–VA, monolayer InN exhibits planar (PL) hexagonal structure like graphene while others (InX (X = P, As, Sb, and Bi)) show low buckled (LB) hexagonal structure like silicene. The InX (X = P, As, Sb, and Bi) are found to have significantly lower

*Project supported by the National Natural Science Foundation of China (Grant Nos. 61675032 and 11604019) and the National Basic Research Program of China (Grant No. 2014CB643900).

†Corresponding author. E-mail: quheruge@bupt.edu.cn
‡Corresponding author. E-mail: photon.bupt@gmail.com

© 2018 Chinese Physical Society and IOP Publishing Ltd

thermal conductivities than InN, because of the strong coupling between out-of-plane modes and in-plane modes. For TE properties, we also investigate their temperature dependence, showing that ZT values increase with temperature rising from 300 K up to 900 K. Finally, we obtain a maximal ZT value of 0.779 for PL structural InN, which is mainly determined by high power factor.

2. Computational methods

We start with investigating structural stability and electronic properties of 2D hexagonal In–VA materials by using the first-principles method as implemented in Vienna *ab-initio* Simulation Package (VASP)[29] code within the framework of the density functional theory (DFT). Perdew–Burke–Ernzerhof (PBE) within the generalized gradient approximation (GGA)[30] is employed to calculate the exchange–correlation potential. The cut-off energy is set to be 400 eV. A Monkhorst–Pack k-mesh of $30\times30\times1$ is used to sample the Brillouin zone (BZ) in reciprocal space during structural relaxation for the unit cell, with limiting to an energy convergence precision of 1×10^{-8} eV and a force convergence precision of 1×10^{-6} eV/Å. For electronic properties, a denser k-point grid of $40\times40\times1$ is employed after structural optimization.

In order to identify the dynamical stabilities of 2D hexagonal In–VA materials, we calculate their phonon spectra based on the force-constant approach with the package of Phonopy.[31] We compute the second-order harmonic interatomic force constants (IFCs)[32] by using the $7\times7\times1$ supercells with k-point meshes of $5\times5\times1$. The electronic coefficients are calculated by using semi-classical Boltzmann transport theory with the relaxation time approximation as implemented in the BoltzTraPl.[33] We obtain the Seebeck coefficient S which is independent of the relaxation time τ, the electrical conductivity σ and the electronic thermal conductivity κ_e which are are divided by relaxation time τ. By applying ShengBTE code,[34] we calculate the third-order anharmonic IFCs. The supercells are defined as $6\times6\times1$ containing 72 atoms with k-point meshes of $5\times5\times1$.

3. Results and discussion

3.1. Structural and electronic properties

We cleave the initial structures of the 2D In–VA materials from the (110) face of the ZB semiconductor In–VA compounds. The atomic structures and lattice constants of the cleaved 2D structures then are both fully optimized. Figure 1 shows 2D planar and buckled honeycomb structures of In–VA. The array of atoms of PL InN resembles the honeycomb hexagonal structure of graphene, forming a planar layer with an In atom and an N atom bonded in a single plane and their π–π bonding is quite strong. In their stable states, other InX (X = P, As, Sb, Bi) form buckled hexagonal structures, since they tend to be more energetic for sp^3 hybridization. The group-III elements In can form trigonal sp^2 bonded molecular structure of the plane with D_{3h} symmetry, while the most common configuration for the group-V elements is of trigonal pyramid.[23] In general, the nature of InN is sp^2 hybridized, however, the heavier group-V elements P, As, Sb, and Bi elements exhibit the sp^2–sp^3 hybridization due to their preference for sp^3 bonding.

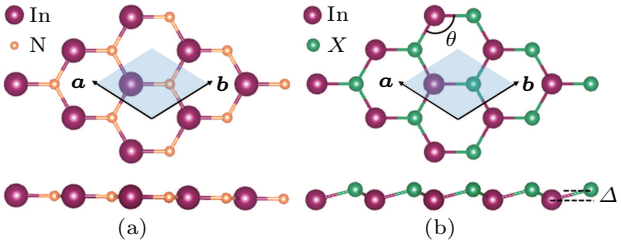


Fig. 1. (color online) Top and side views for 2D (a) planar InN and (b) buckled honeycomb InX (X = P, As, Sb, Bi) structures. In the planar structure, atoms are located on the same plane. In the buckled structure, the alternating atoms are located in two different parallel planes. The buckling Δ is the distance between these two planes. θ refers to the value of angle between neighboring bonds.

Table 1. Calculated structural and electrical properties of 2D hexagonal In–VA. Stable structures are identified as planar and buckled geometries, respectively, showing the values of lattice constant (a), buckling parameter (Δ), angle between neighboring bonds (θ), energy gap (E_g), calculated within PBE. The electron effective mass,m_e^*/m_0, θ, and Δ are described in Fig. 1.

	a/Å	Δ/Å	θ/(°)	m_e^*/m_0	E_g/eV
InN	3.57	0	120	0.54	0.46
	3.63[a]			0.43[a]	
	3.57[b]				
InP	4.25	0.54	115.51	0.44	1.16
	4.25[a]	0.52[a]		0.37[a]	
	4.17[b]	0.51[b]	115.8[b]		
InAs	4.38	0.67	113.60	0.41	0.85
	4.38[a]	0.67[a]		0.32[a]	
	4.28[b]	0.62[b]	114.1[b]		
InSb	4.68	0.77	112.82	0.33	0.79
	4.68[a]	0.76[a]		0.28[a]	
	4.57[b]	0.73[b]	113.2[b]		
InBi	4.80	0.85	111.76	0.25	0.17
	4.81[c]	0.85[c]			

[a]Ref. [23], [b]Ref. [24], [c]Ref. [35].

Figure 1(a) illustrates this PL hexagonal structure of InN with space group PM2, and figure 1(b) shows the low-buckled (LB) hexagonal nature of InX with space group P3M1. Each group-V atom is covalently bonded with one In atom, forming a simple hexagonal unit cell. For LB structure, atoms of In and VA lie in different planes having a buckling distance, Δ, as shown in Fig. 1(b). The obtained equilibrium lattice constant a_0 and buckling height Δ are listed in Table 1.

The calculated values of equilibrium lattice constant a_0 in LB phase of InP, InAs, InSb, and InBi are 4.25 Å, 4.38 Å, 4.68 Å, and 4.80 Å for the pristine buckled honeycombs, which are all larger than 3.57 Å of InN. In buckled geometries, as the position of In atom rises, the value of angle between neighboring bonds VA–In–VA decreases. These structural properties are in good agreement with those of previous theoretical work.[23,24,35] To date, there have been no theoretical or experimental results about the structural or electrical transitions of 2D In–VA in our investigated temperature range. Therefore, the obtained structures here are used for calculating the TE properties below.

The calculated band structures of single-layer In–VA and their corresponding total densities of states (DOSs) are plotted in Figs. 2 and 3, respectively. At the PBE level, the bottom of the conduction band is located at Γ point. Single-layered InN and InP are predicted to be indirect-band-gap semiconductors with band gaps of 0.46 eV and 1.16 eV, respectively. The InAs, InSb, and InBi are direct-band-gap semiconductors with band gaps of 0.85 eV, 0.79 eV, and 0.17 eV, respectively, following a decreasing trend. For InX with buckling height, the energy band gap shrinks as atomic number increases.

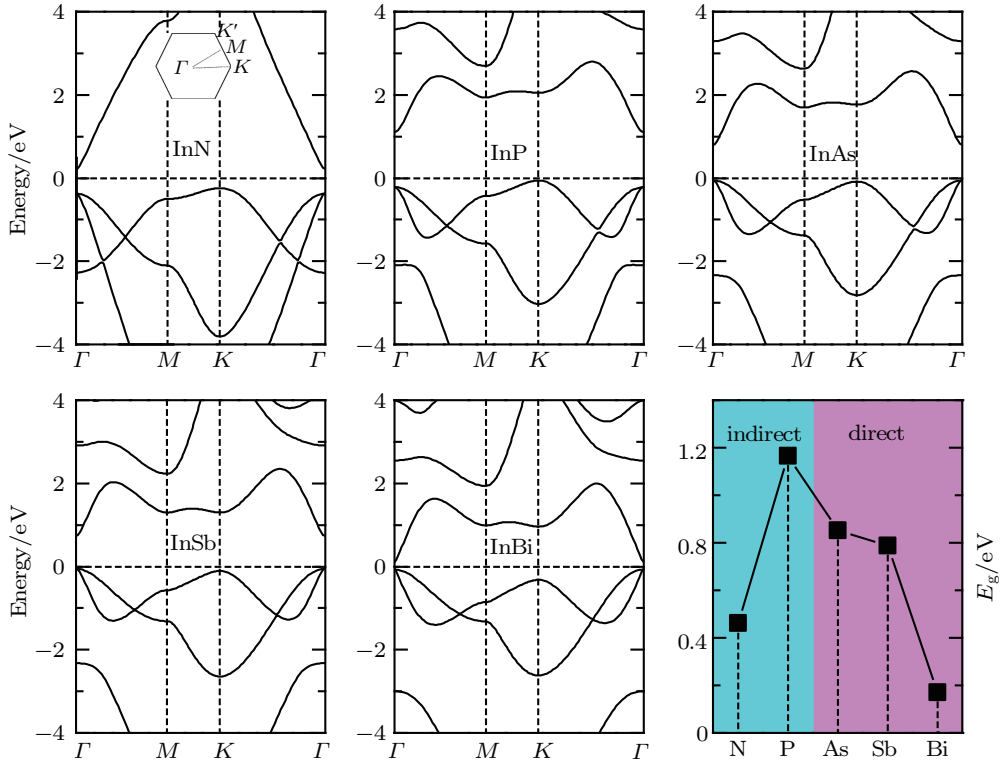


Fig. 2. (color online) Energy bands of monolayer honeycomb structures of In–VA.

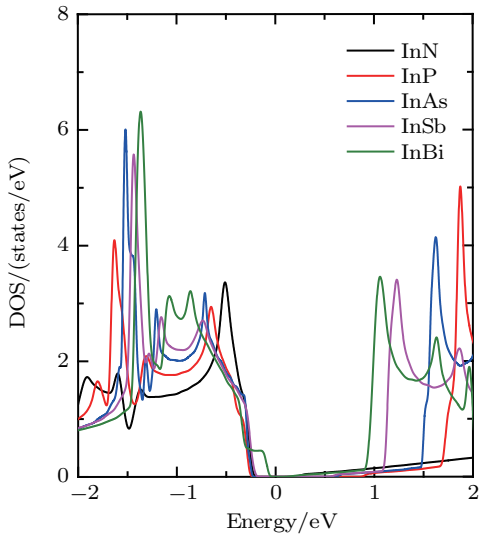


Fig. 3. (color online) Total DOSs of In–VA around the Fermi level.

Figure 3 shows the total DOSs for all five In–VA compounds near the Fermi level, which are mainly associated with TE properties.[36] Due to the total DOS increasing more rapidly near the VBM than near the CBM, thermal power factors for p-type cases will be much larger than for n-type cases. Dramatic DOS variation near the VBM is favorable for high Seebeck coefficients.[37] Sharp peaks in the electronic DOS near the Fermi energy can enhance the TE performances in monolayer systems, which could partially be attributed to the improving electrical conductivity and imposing asymmetry between holes and electrons transport.[38,39]

3.2. Phonon dispersion and stability

The dynamical stability of the hexagonal 2D In–VA is determined by the phonon spectra shown in Fig. 4. None of the five In–VA materials shows imaginary frequencies,

demonstrating that all the structures are dynamically stable. The lattice thermal conductivity is mainly governed by anharmonic phonon–phonon scattering.[40] It is one optical branch of InN that has low frequencies and overlaps with the acoustic branches, which is different from LB structural InX, and can be seen as an indication of soft mode and strong anharmonicity.[41] Consequently, low thermal conductivities are obtained. The optical branches of the LB InX structures move gradually to lower frequencies, as the atomic number of X increases. The main reason for the production of different flexural phonon modes is anticipated to be due to the buckling structures in InP, InAs, InSb, and InBi, which leads to strong coupling between out-of-plane modes and in-plane modes. Besides, the strengths of In–X (X = P, As, Sb, Bi) bonds are much weaker than those of the In–N bonds, leading to a significantly lower group velocity of the ZA mode in InX.

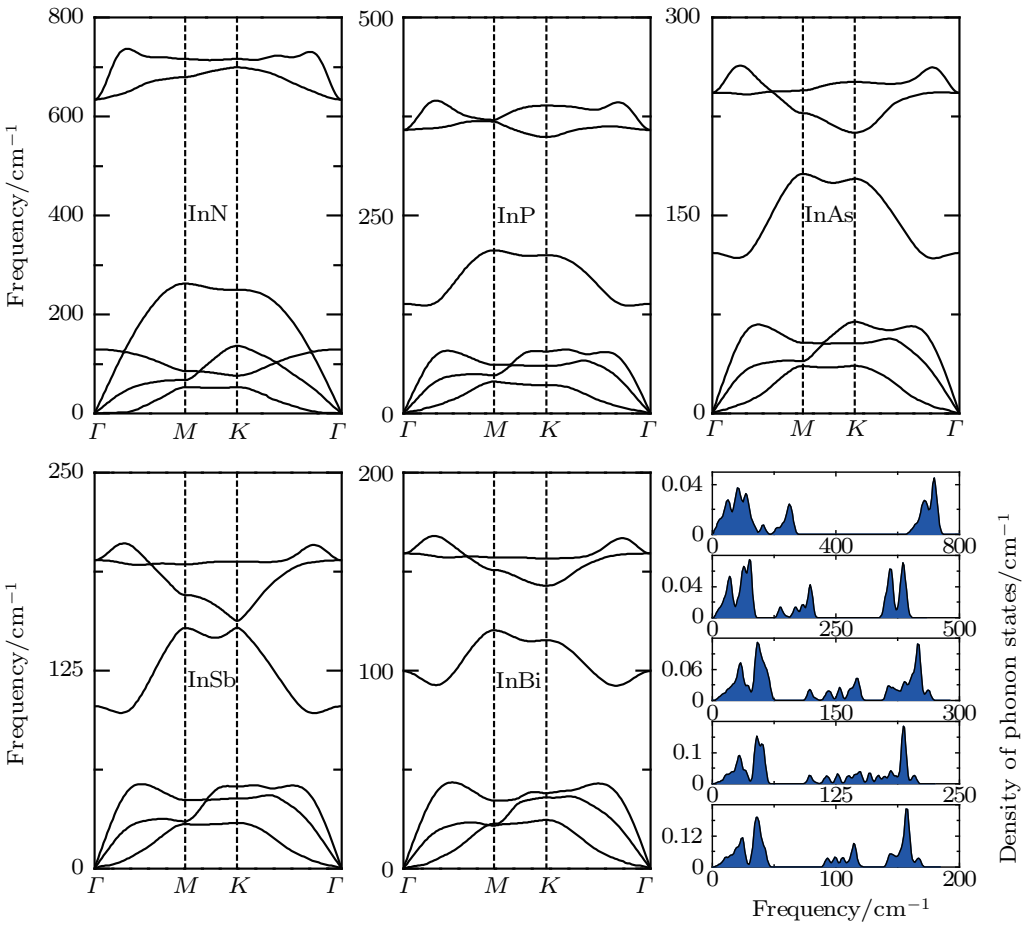


Fig. 4. (color online) Calculated vibration frequencies of phonon modes versus k of monolayer In–VA.

3.3. TE properties

According to the calculated electronic structures, we are able to evaluate the electronic transport coefficients by using the Boltzmann transport equation within constant relaxation time approximation. The Seebeck coefficient S can be calculated to be independent of the relaxation time τ, while the electrical conductivity σ is divided by τ, so what we obtain is σ/τ. The relaxation time is usually obtained by fitting to the experimental data.[42] Since there are no clear experimental values against which these compounds can be measured, we assume $\tau = 2 \times 10^{-14}$ s in the present calculations, which is reasonable.[43] The Seebeck coefficient S and electrical conductivity σ are given by[44,45]

$$\sigma_{\alpha\beta}(T,\mu) = \frac{1}{\Omega}\int \sigma_{\alpha\beta}(\varepsilon)\left[-\frac{\partial f_\mu(T,\varepsilon)}{\partial\varepsilon}\right]\mathrm{d}\varepsilon, \quad (1)$$

$$S_{\alpha\beta}(T,\mu) = \sum_\gamma (\sigma^{-1})_{\alpha\gamma}\nu_{\beta\gamma}, \quad (2)$$

where e is the charge of electron, f_μ is the Fermi distribution function, μ is the chemical potential, ε is the band energy, T is the absolute temperature, and τ is the relaxation time. Seebeck coefficient is inversely proportional to the carrier concentration, while electrical conductivity is proportional to carrier concentration.[46]

The Seebeck coefficients of the single-layer In–VA as a function of chemical potential (μ) at different temperatures are plotted in Fig. 5(a). The positive and negative μ correspond to n-type and p-type doping of the system, respectively. As ex-

pected, under n-type and p-type doping, S, σ/τ, and PF/τ are all enhanced. In Fig. 5(a), a sharp change with two opposite peaks of Seebeck coefficients around the Fermi level occurs, and there is a downward trend in the value of S with the increase of the temperature T, indicating that an optimal carrier concentration is favorable for improving TE performance. The peak values of Seebeck coefficient at room temperature are 1015 μV/K for the InN single-layer, 1786 μV/K, 1396 μV/K, 1272 μV/K, and 289 μV/K, for the LB InX single-layer, respectively, which are all for the p-type doping. It is seen that S plots of In–VA are asymmetric for p-type and n-type doping, and the former is more preferable, which may be due to the asymmetry of valence and conduction bands of In–VA.

In Fig. 5(b), σ/τ increases gradually with the changing of chemical potential near Fermi level. When the doping level is relatively small, with band gap increasing, σ/τ generally decreases in similar manners and close values, which is in contrast to the tendency of the Seebeck coefficient. The highest value of σ/τ is attained for InBi in the vicinity of fermi level. This behavior can be attributed to a small effective mass associated with InBi. Unlike the Seebeck coefficients, electrical conductivities are less sensitive to temperature. For the p-type doped In–VA monolayer, the electrical conductivities are significantly increased with the doping level, which are larger than those of the n-type ones.

In Fig. 5(c), we plot the power factors of the In–VA monolayer under the conditions of different chemical potentials and temperatures. In the case of chemical potential, the maximum PF generally increases with band gap decreasing, which could be attributed to the increased electrical conductivity exceeding the negative effect of the Seebeck coefficients. The PF is larger for p-type doping level than for n-type doping level for both PL and LB monolayer systems and will increase with doping level increasing. At the same time, the high DOS near Fermi energy provides large enough electrical conductivity. Consequently, the PF ($S^2\sigma$) of the single-layered PL InN shown in Fig. 5(c) is larger than that of LB InX materials.

The electronic thermal conductivity is addressed in Fig. 5(d). As expected, these values increase with the increase of doping level and the temperature, showing a similar trend to that of electrical conductivity σ. The effect of temperature on electronic thermal conductivity is more apparent than on electrical conductivity.

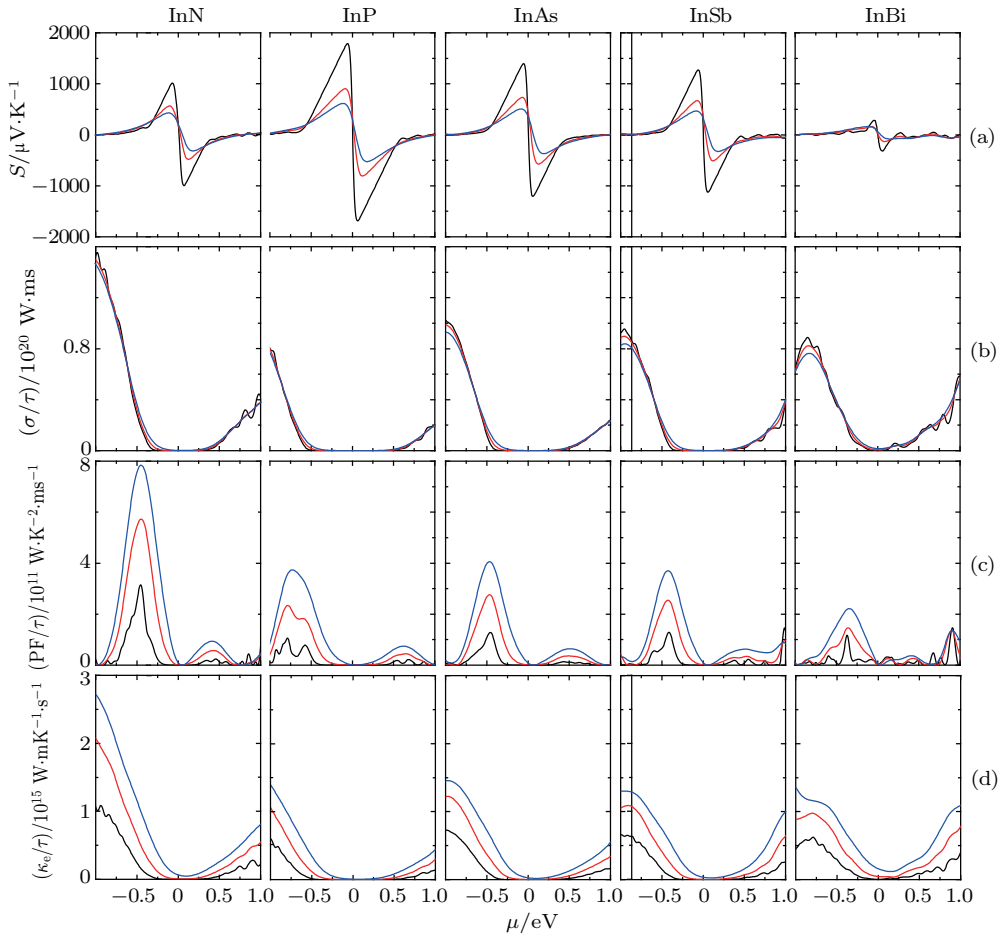


Fig. 5. (color online) Calculated TE properties: (a) Seebeck coefficients, (b) electrical conductivities, (c) power factors, and (d) electrical thermal conductivities relative to relaxation time, of 2D InX as a function of chemical potential at 300 K (black line), 600 K (red line), and 900 K (blue line), respectively.

Next, we will investigate the doping effect on the thermal transport property of the In–VA monolayer. The intrinsic lattice thermal conductivities of the single-layered In–VA at different temperatures are estimated by using the ShengBTE[35] code based on the phonon Boltzmann transport equation, and the results are shown in Fig. 6. For both cases, κ_l decreases with the reciprocal of temperature (T^{-1}) increasing. This implies that the dominant scattering mechanism is the Umklapp process.[38] The lattice thermal conductivity of PL InN is evidently larger than that of the LB structure. From InP to InBi, with the increasing of buckling height and decreasing of phonon scattering, the lattice thermal conductivities diminish.

With all the transport coefficients available, ZT values of the single-layered In–VA as a function of chemical potential at different temperatures are obtained as shown in Fig. 7. At 900 K, the ZT values reach the maximum values for In–VA whether it is PL or LB structure, at p-type doping levels. The maximal ZT values of 0.779, 0.583, 0.696, 0.727, and 0.373 for InN, InP, InAs, InSb, and InBi are observed at $\mu = -0.306$ eV, $\mu = -0.449$ eV, $\mu = -0.281$ eV, $\mu = -0.231$ eV, and $\mu = -0.232$ eV, respectively. Attributed to the p-type, the doped power factors are greater than the n-type doped ones, and p-type doped ZT values of In–VA are higher than those of n-type doping levels. Thus the properly p-type doped In–VA should be potential TE materials working at medium-high temperature.

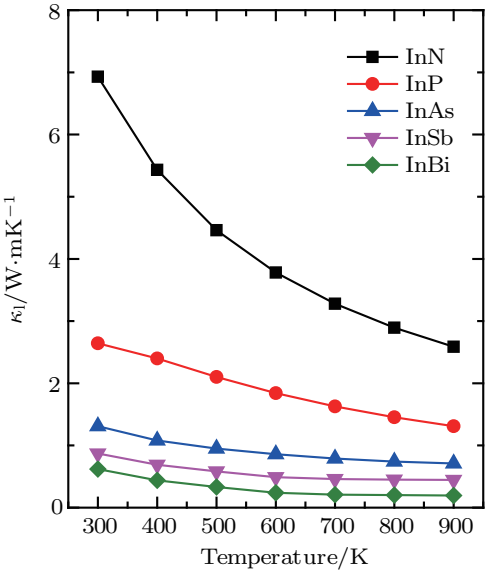


Fig. 6. (color online) Lattice thermal conductivities of 2D In–VA as a function of temperature, from 300 K to 900 K.

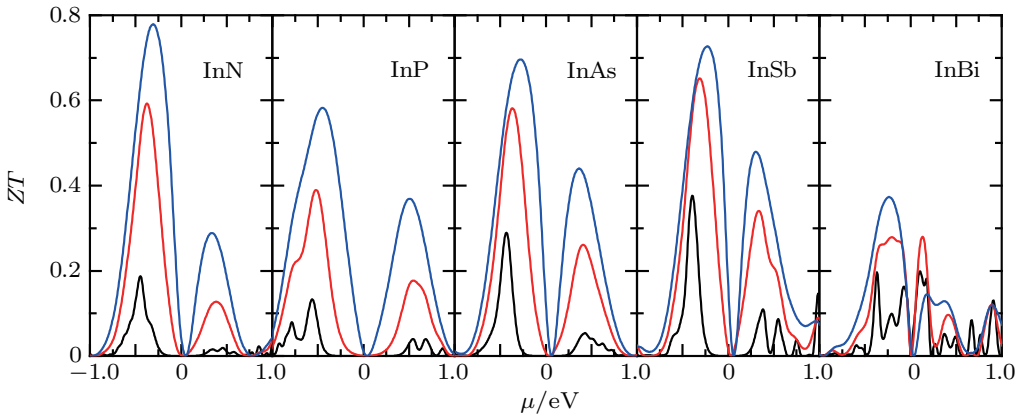


Fig. 7. (color online) ZT values as a function of the carrier concentration of the In–VA monolayer at 300 K (black line), 600 K (red line), and 900 K (blue line), respectively.

3.4. Temperature dependence

In order to investigate TE properties and their temperature relationships of In–VA more intuitively, we plot Seebeck coefficients, electrical conductivities, PF trend, ZT values versus temperature at a carrier density of 4.8×10^{20} cm^{-3} as shown in Fig. 8.

Figure 8(a) illustrates the tendencies of the Seebeck coefficients, which increase with temperature rising. Our measurements of Seebeck coefficients consistently indicate that appropriate doping to In–VA induces electron carriers, beneficial to the improvement of the TE performance. There is a slightly downward trend in the value of σ/τ with the increase of temperature which is opposite to the trend of the Seebeck coefficient. Increased electron carrier concentration due to p-type doping is responsible for high electrical conductivity in In–VA. At the same doping level and same temperature, InN which possesses the maximal electron effective mass exhibits the biggest Seebeck coefficient and the smallest electrical conductivities in these five materials. Figure 8(c) shows the PF with the constant relaxation time, which is used to calculate the ZT value. In relatively highly p-type doped samples, we observe that PF increases with temperature rising up to 900 K.

The ZT values as a function of temperature are shown in Fig. 8(d). The maximum ZT values of In–VA are 0.779, 0.504, 0.554, 0.494, and 0.308 at 900 K with carrier densities being all 4.8×10^{20} cm^{-3}, respectively. For the p-type doping, the maximal ZT value of InN is larger than that of LB structural InX, which is mainly attributed to the prominently maximal S (about 283 μV/K at 900 K) in this case. It is observed that the

maximal ZT value of In–VA at 900 K is much larger than that at 300 K with the corresponding doping concentration, which is caused due to the increase of the electrical conductivity and the decrease of the lattice thermal conductivity with the increase of temperature. It manifests that 2D In–VA is indeed a medium-high temperature TE material.

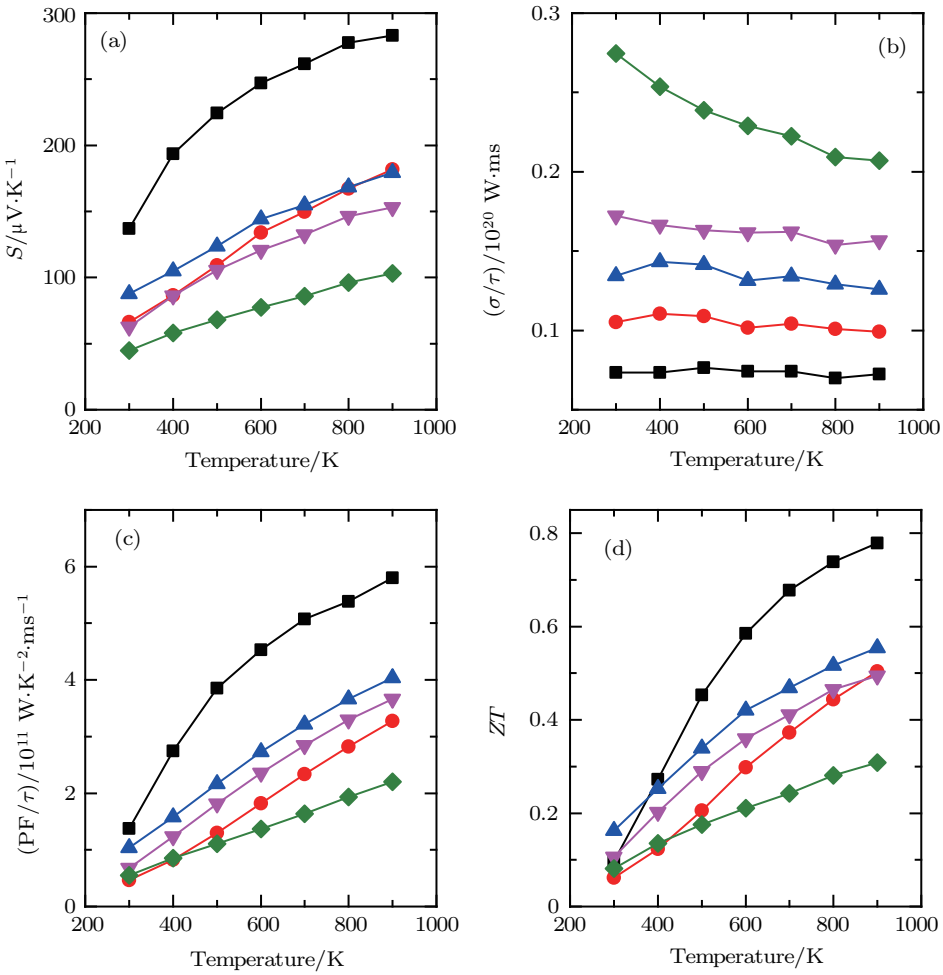


Fig. 8. (color online) Calculated TE properties: (a) Seebeck coefficients, (b) electrical conductivities, (c) power factors relative to relaxation time, and (d) ZT, of 2D InN (black lines), InP (red lines), InAs (blue lines), InSb (pink lines), and InBi (green lines) as a function of temperature, respectively.

4. Conclusions

Using *ab initio* calculations, electronic properties of In–VA in monolayer form are studied, and TE properties are analyzed by using Boltzmann transport equations for the electrons and phonons. The TE response of InN turns out to be superior to those of InX (X = N, P, As, Sb, Bi), and the origin of this difference is ascertained to be relevant to the structural and electronic properties. The ultralow intrinsic thermal conductivities of 2.64 W·m^{-1}·K^{-1}(InP), 1.31 W·m^{-1}K^{-1} (InAs), 0.87 W·m^{-1}·K^{-1} (InSb), and 0.62 Wm^{-1}·K^{-1} (InBi) evaluated at room temperature are close to the typical thermal conductivities of good TE materials ($\kappa < 2$ W·m^{-1}·K^{-1}). The high figures of merit of monolayer In–VA in a wide temperature range are interesting from the point of view of application. The present study not only provides various unexpected properties of In–VA, but also gives the hints that it could be used to explore the TE effects of the 2D III–V materials.

Acknowledgement

We are indebted to the Beijing Computational Science Research Center for computing service.

References

[1] Novoselov K S, Geim A K, Morozov S V, Dubonos S V, Zhang Y and Jiang D 2004 *Science* **306** 660
[2] Zhi C, Bando Y, Tang C, Kuwahara H and Golberg D 2009 *Adv. Mater.* **21** 2889
[3] Nag A, Raidongia K, Hembram K P, Datta R, Waghmare U V and Rao C N R 2010 *ACS Nano* **4** 1539
[4] Li L, Yu Y, Ye G J, Ge Q, Ou X, Wu H, Feng D, Chen X and Zhang Y 2014 *Nat. Nanotechnol.* **9** 372
[5] Liu H, Neal A T, Zhu Z, Luo Z, Xu X, Tománek D and Peide D Y 2014 *ACS Nano* **8** 4033
[6] Jing Y, Zhang X and Zhou Z W 2016 *Wiley Interdiscip. Rev. Comput. Mol. Sci.* **6** 5
[7] Aufray B, Kara A, Vizzini S, Oughaddou H, Léandri C, Ealet B and Le Lay G 2010 *Appl. Phys. Lett.* **96** 183102
[8] Kara A, Enriquez H, Seitsonen A P, Voon L L Y, Vizzini S, Aufray B and Oughaddou H 2012 *Surf. Sci. Rep.* **67** 1
[9] Vogt P, De Padova P, Quaresima C, Avila J, Frantzeskakis E, Asensio M C, Resta A, Ealet B and Le Lay G 2012 *Phys. Rev. Lett.* **108** 155501

[10] Zhang G and Zhang Y W 2015 *Mech. Mater.* **91** 382
[11] Dragoman D and Dragoman M 2007 *Appl. Phys. Lett.* **91** 203116
[12] Matusalem F, Marquez M, Teles L K and Bechstedt F 2015 *Phys. Rev. B* **92** 045436
[13] Zhang G and Zhang Y W 2017 *Chin. Phys. B* **26** 034401
[14] Sztein A, Ohta H, Sonoda J, Ramu A, Bowers J E, DenBaars S P and Nakamura S 2009 *Appl. Phys. Express* **2** 111003
[15] Kaiwa N, Hoshino M, Yagainuma T, Izaki R, Yamaguchi S and Yamamoto A 2007 *Thin Solid Films* **515** 4501
[16] Pantha B N, Dahal R, Li J, Lin J Y, Jiang H X and Pomrenke G 2008 *Appl. Phys. Lett.* **92** 042112
[17] Yamaguchi S, Iwamura Y and Yamamoto A 2003 *Appl. Phys. Lett.* **82** 2065
[18] Tong H, Zhao H, Handara V A, Herbsommer J A and Tansu N 2009 *Proc. SPIE - Int. Soc. Opt. Eng.* **6** 309
[19] Sztein A, Haberstroh J, Bowers J E, DenBaars S P and Nakamura S 2013 *J. Appl. Phys.* **113** 183707
[20] Goyal V, Teweldebrhan D and Balandin A A 2010 *Appl. Phys. Lett.* **97** 133117
[21] Fan Z, Zheng J, Wang H Q and Zheng J C 2012 *Nanoscale Res. Lett.* **7** 570
[22] Cheng Y, Yang J, Jiang Q, He D, He J, Luo Y, Zhang D, Zhou Z, Ren Y and Xin J 2017 *J. Mater. Chem. A* **5** 5163
[23] Zhuang H L, Singh A K and Hennig R G 2013 *Phys. Rev. B* **87** 165415
[24] Şahin H, Cahangirov S, Topsakal M, Bekaroglu E, Akturk E, Senger R T and Ciraci S 2009 *Phys. Rev. B* **80** 155453
[25] Singh A K, Zhuang H L and Hennig R G 2014 *Phys. Rev. B* **89** 245431
[26] Watanabe K, Taniguchi T and Kanda H 2004 *Nat. Mater.* **3** 404
[27] Tsipas P, Kassavetis S, Tsoutsou D, Xenogiannopoulou E, Golias E, Giamini S A, Grazianetti C, Chiappe D, Molle A, Fanciulli M and Dimoulas A 2013 *Appl. Phys. Lett.* **103** 251605
[28] Huang Z, Lü T Y, Wang H Q, Yang S W and Zheng J C 2017 *Comput. Mater. Sci.* **130** 232
[29] Kresse G and Furthmüller J 1996 *Phys. Rev. B* **54** 11169
[30] Perdew J P, Burke K and Ernzerhof M 1996 *Phys. Rev. Lett.* **77** 3865
[31] Togo A, Oba F and Tanaka I 2008 *Phys. Rev. B* **78** 134106
[32] Li W, Lindsay L, Broido D A, Stewart D A and Mingo N 2012 *Phys. Rev. B* **86** 174307
[33] Madsen G K and Singh D J 2006 *Comput. Phys. Commun.* **175** 67
[34] Li W, Carrete J, Katcho N A and Mingo N 2014 *Comput. Phys. Commun.* **185** 1747
[35] Crisostomo C P, Yao L Z, Huang Z Q, Hsu C H, Chuang F C, Lin H, Albao M A and Bansil A 2015 *Nano Lett.* **15** 6568
[36] Ding G, Gao G Y and Yao K L 2014 *J. Phys. D: Appl. Phys.* **47** 385305
[37] Hong A J, Li L, Zhu H X, Yan Z B, Liu J M and Ren Z F 2015 *J. Mater. Chem. A* **3** 13365
[38] Wang F Q, Zhang S, Yu J and Wang Q 2015 *Nanoscale* **7** 15962
[39] Kumar Sand Schwingenschlögl U 2015 *Chem. Mater.* **27** 1278
[40] Ziman J M 1960 *Electrons and Phonons: The theory of Transport Phenomena in Solids* (Oxford: Oxford University Press)
[41] Yang J, Yuan Q, Deng H X, Wei S H and Yakobson B I 2017 *J. Phys. Chem. C* **121** 123
[42] Yu J, Sun Q and Jena P 2016 *International Symposium on Clusters and Nanomaterials*, pp. 101740C–101740C
[43] D'Souza R and Mukherjee S 2016 *J. Phys. Conf. Ser.* **759** 12040
[44] Zhang L and Singh D J 2010 *Phys. Rev. B* **81** 245119
[45] Guan X, Lu P, Wu L, Han L, Liu G, Song Y and Wang S 2015 *J. Alloys Compd.* **643** 116
[46] Li H Z, Li R P, Liu J H and Huang M J 2015 *Physica B: Condens. Matter* **479** 1